GA–A22643

IMPROVED ENERGY CONFINEMENT WITH NEON INJECTION IN THE DIII–D TOKAMAK

by
G.M. STAEBLER, G.L. JACKSON, W.P. WEST, S.L. ALLEN,
R.J. GROEBNER, M.J. SCHAFFER, and D.G. WHYTE

JUNE 1997

DISCLAIMER

GA–A22643

IMPROVED ENERGY CONFINEMENT WITH NEON INJECTION IN THE DIII–D TOKAMAK

by
G.M. STAEBLER, G.L. JACKSON, W.P. WEST, S.L. ALLEN,[†]
R.J. GROEBNER, M.J. SCHAFFER, and D.G. WHYTE[‡]

This is a preprint of a paper to be presented at the Twenty-Fourth European Conference on Controlled Fusion and Plasma Physics, June 9–14, 1996, Berchtesgaden, Germany, and to be published in the *Proceedings*.

[†]Lawrence Livermore National Laboratory
[‡]University of California, San Diego

Work supported by
the U.S. Department of Energy
under Contract No. DE-AC03-89ER51114,
and Grant No. DE-FG03-95ER54294

GA PROJECT 3466
JUNE 1997

IMPROVED ENERGY CONFINEMENT WITH NEON INJECTION IN THE DIII–D TOKAMAK*

G.M. Staebler, G.L. Jackson, W.P. West, S.L. Allen,† R.J. Groebner, M.J. Schaffer, and D.G. Whyte‡

General Atomics, P.O. Box 85608, San Diego, California, 92186-5608 USA

In this paper we will report the first direct measurements of the fully stripped neon 10^+ density profile in a plasma with enhanced energy confinement due to neon injection. This is made with a calibrated charge exchange recombination (CER) system [1]. It is found that the neon 10^+ density is peaked like the electron density with a slightly higher concentration towards the edge. The good news is that the neon 10^+ fraction is less than 1% (normalized to the electron density). The radial electric field can also be computed from the CER measurements on DIII–D. The shear in the E×B velocity is found to exceed the maximum growth rate of the ion temperature gradient (ITG) mode over part of the profile, a condition for the suppression of turbulent transport [2]. This agrees with the reduced power balance thermal diffusivities near the magnetic axis.

The phenomenon of enhanced energy confinement in tokamaks during impurity injection and auxiliary heating has been observed on several tokamaks. ISX-B had the Z–mode [3], TEXTOR the I–mode [4] and JFT-2M the IL–mode [5]. TEXTOR can get the I–mode without seeding impurities at low density, but the best performance has been with neon injection at high density and high radiated power (RI–mode) [6]. All of these enhanced confinement regimes have peaked density profiles, high auxiliary heating, high radiation, usually due to neon but other impurities have also been successful, and no sawteeth. TEXTOR has found sawtoothing RI–modes. JFT-2M has reported IL–modes with both limiters and divertors. Energy confinement times for IL–mode in JFT-2M were as good or better than the preceding ELM-free H–mode. Sawtoothing discharges with modest energy confinement improvement (1.5 times L–mode)have been observed on ASDEX-U [7] when neon injection has suppressed the H–mode. About two dozen DIII–D discharges with L–mode edges and strong neon radiation have been produced with energy confinement up to 2.0 times L–mode but most with 1.4–1.6 times L–mode. All but the highest one reported here were sawtoothing. A variety of configurations are represented, both double null and single null topologies and both ion ∇B drift toward and away from the dominant X–point. We will adopt the IL–mode terminology for these plasmas. A few discharges which returned to an H–mode edge after an IL–mode phase have been observed. In this paper we will present analysis of a plasma which obtains an energy confinement three times L–mode before sawteeth and ELMs set in returning the energy confinement to a normal H–mode level. This discharge retains the improved core confinement of the preceding IL–mode but adds on the H–mode edge barrier. This type of regime will be referred to as an IH–mode.

A single discharge with both an IL– and IH–mode phase will be analyzed in this paper. An overview of DIII–D discharge 86457 is given in Fig. 1. This was a lower single null plasma with the ion ∇B drift towards the X–point The divertor cyropump was active but the outer strike point was not located for maximizing pumping. Other parameters are: toroidal field 1.77 T, plasma current

*Work supported by U.S. Department of Energy under Contract No. DE-AC03-89ER51114 and Grant No. DE-FG03-95ER54294.

†Lawrence Livermore National Laboratory.

‡Univeristy of California, San Diego.

1.28 MA, minor radius 0.60 m, major radius 1.70 m, elongation 1.85. Neutral beam power (4.0 MW) began at 1.0 s yielding an H–mode transition 80 ms later. A neon gas puff was injected from 1.2–1.4 s and the plasma remained ELM free until a few large ELM bursts and an H to L transition occurred due to the large radiated power. Beginning at about 1.6 s the drop in stored energy halted. At this point the energy confinement time was 110 ms which is 1.2 times L–mode (ITER 89p scaling [8] including the stored energy time derivative correction to the beam plus Ohmic power). This marks the start of the IL–mode phase. The stored energy continues to climb until a transition to IH–mode at 1.92 s At 1.87 s the energy confinement has reached 234 ms. (2.0 times L–mode). During the IH–mode phase the energy confinement increases reaching a peak of 382 ms or 3.1 times L–mode at 2.1 s. The energy confinement time is above 2.5 times L–mode for most (1.94–2.2 s) of the IH–mode phase. The stored energy returns to its pre-neon puff level (energy confinement 2 times L–mode) after the onset of steady ELMs and sawteeth beyond 2.4 s. The sawteeth were delayed by the injection of one neutral beam during the current ramp-up. The safety factor (q) profile (measured with a motional stark effect diagnostic) is monotonic with positive shear but is somewhat above one at the center (see insert in Fig. 5). The profiles of the ion and electron temperature, the electron density and neon 10^+ density are shown in Fig. 2 at 1.6, 1.9 and 2.2 s. During the IL–mode phase (from 1.6 to 1.9 s) the electron and ion temperatures rise but the electron density is nearly unchanged. The neon 10^+ concentration becomes slightly hollow. After the transition to IH–mode, the electron and ion temperatures broaden as the edge density rises sharply. In the early IH–mode phase the temperatures remain more centrally peaked. The dramatic rearrangement of the neon 10^+ profile between the 1.9 and 2.2 s begins immediately after the IH–mode transition. Because of the rise in the edge electron density the neon 10^+ concentration relative to electron density is not nearly as hollow as the neon 10^+ density. The neon 10^+ concentration is more hollow in IH–mode

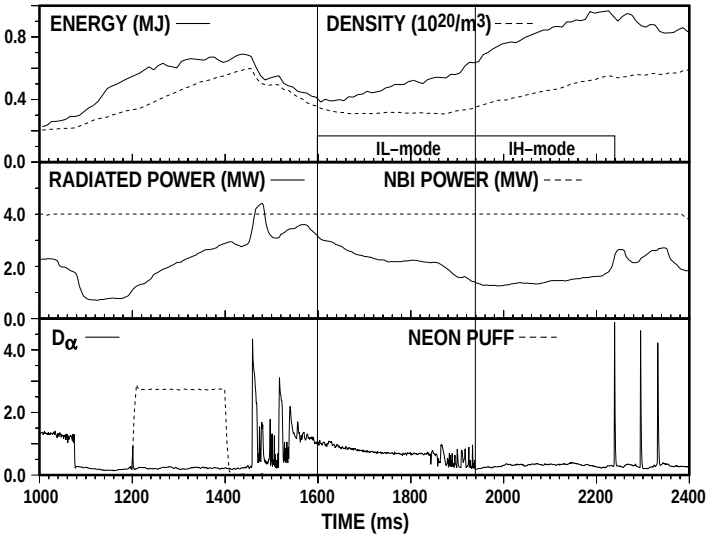

Fig. 1. DIII–D discharge 86457 overview showing stored energy, line-averaged density, total radiated power, neutral beam power, divertor D_α light, and the neon gas valve voltage.

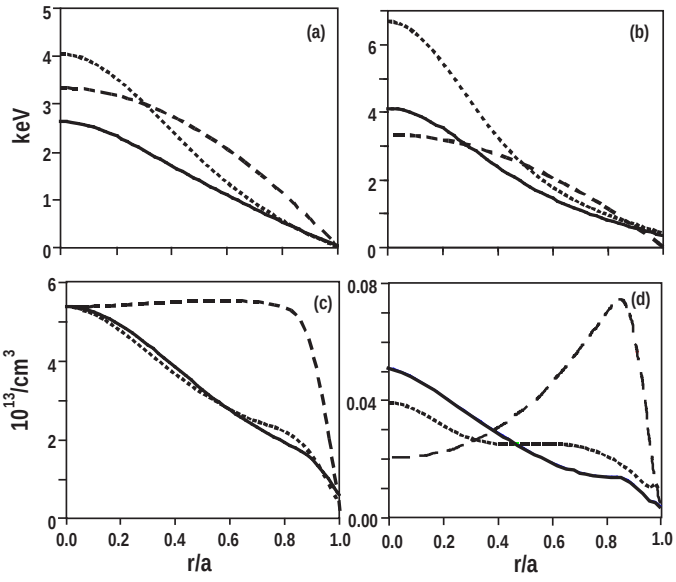

Fig. 2. Measured radial profiles of electron temperature (a), ion temperature (b) electron density (c) and neon 10^+ density (d) at three times: 1.6 s (solid), 1.9 s (dotted), 2.2 s (dashed).

than during the IL–mode phase. The measured neon 10^+ toroidal rotation profile behaves similarly to the ion temperature.

Transport analysis of this discharge has been made with the ONETWO code. Experimental profiles and EFIT equilibria were taken every 50 ms from 1.6 to 2.2 s. The profiles were then smoothed in time using a boxcar average over 150 ms intervals. The electron thermal diffusivity profiles at several times are shown in Fig. 3. The electron thermal diffusivity first falls near the center and then the reduction propagates towards the edge during the IL–mode phase. (1.6, 1.8, 1.9 s). The IH–mode phase begins with a reduction near r/a = 0.8 retaining the low central transport initially (2.1 s). Late in the IH–mode phase (2.2 s) the central electron thermal diffusivity has risen above its value at 1.6 s. The ion thermal diffusivity profiles are shown in Fig. 4 along with the ion neoclassical [9] thermal diffusivity at 2.2 s. The ion thermal diffusivity also falls near the axis first during the IL–mode phase. (1.6, 1.8, 1.9) but does not show much reduction farther out until the IH–mode phase (2.2 s) The profile at 2.1 s is the same as at 2.2 s. The persistence of a region with a power balance ion thermal diffusivity below standard neoclassical may be consistent with a revised neoclassical theory [10].

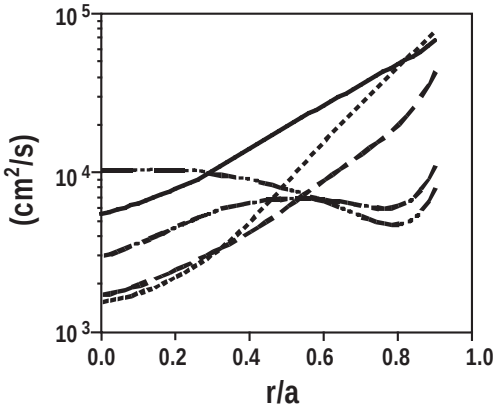

Fig. 3. Power balance electron thermal diffusivity profiles at five times: 1.6 s (solid), 1.8 s (dotted), 1.9 s (dot dashed), 2.1 s (dashed), 2.2 s (dot dot dashed).

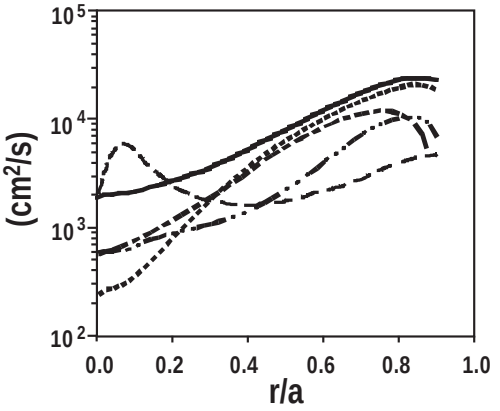

Fig. 4. Power balance ion thermal diffusivity profiles at four times: 1.6 s (solid), 1.8 s (dotted), 1.9 s (dot dashed), 2.2 s (dot dot dashed), also shown is the ion neoclassical thermal diffusivity at 2.2 s (dashed).

It has been shown theoretically that E×B velocity shear could yield core transport reduction even when the edge remains in L–mode due to high radiation [11]. In order for the E×B velocity shear to suppress transport it must exceed the maximum growth rate of the turbulent instability [2]. The measured E×B shear rate at 1.9 s and the maximum growth rate for ITG modes is shown in Fig. 5. The growth rate was computed using a comprehensive gyro-kinetic stability code in the ballooning representation [12]. The neon impurity was included in the calculation and the electrostatic approximation was used. The E×B shear exceeds the maximum growth rate in two regions, near the magnetic axis and near r/a=0.7. Both ions and electrons have reduced thermal diffusivities for r/a<0.4 which suggest that the E×B shear could contribute to the improvement in this region. However, the region near r/a=0.7 shows only a reduction in the electron thermal diffusivity at 1.9 s and there is no sign of a dramatic transport barrier with steep gradients in this region. The sharp rise in the growth rate at r/a=0.8 is due to an electron temperature gradient (ETG) mode becoming dominant over the ITG mode. The maximum growth rate for this mode is about 6 MHz at a wavenumber 100 times larger than the ITG mode. The ETG mode is stable for r/a<0.3 so it cannot affect the core but it may be preventing the E×B shear from suppressing the turbulence at r/a=0.7 by driving the ITG mode non-linearly. Even when the

E×B shear does not completely stabilize the turbulence it can reduce transport. The fact that the electron thermal diffusivity shows a broader region of reduction than the ions during the IL–mode is a unique feature of this mode compared to other enhanced core modes (NCS, VH) observed on DIII–D. It is interesting that the core particle transport does not appear to improve. Since the Thomson scattering diagnostic does not give electron density data inside of r/a=0.3 on this discharge it is possible that the density is somewhat more peaked than shown. However, the central electron cyclotron emission radiometer (which measures electron temperature) was not cut-off indicating that the central density was below 8.0×10^{13}.

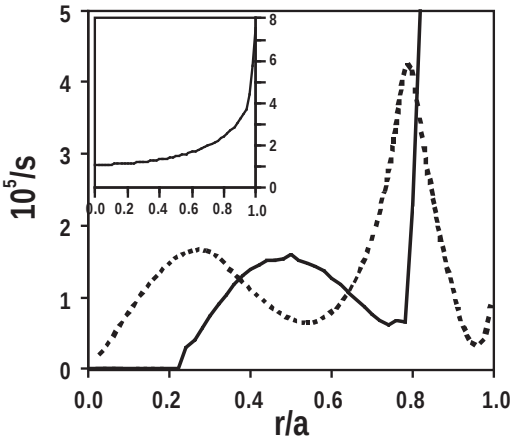

Fig. 5. Profile of the maximum ITG growth rate (solid) and measured E×B shear (dotted) at 1.9 s. Insert shows the measured safety factor profile at 1.9 s.

Both the IL–mode and the IH–mode deserve further study. IH–mode has a lower central impurity concentration and a higher confinement than IL–mode but it may not be able to achieve steady state and the particle confinement may be too good for helium ash removal. The IL–mode has a lower power flow to the divertor and peaked density profiles. It has yet to be demonstrated that E×B shear can produce a transport barrier just inside the radiating mantel as predicted [11] but E×B shear is contributing to the improved energy confinement of IL–mode.

[1] D.G. Whyte *et al.*, "Measurement and Verification of Z_{eff} Radial Profiles Using Charge Exchange Recombination Spectroscopy on DIII–D," to be submitted to Nucl. Fusion.
[2] R.E. Waltz *et al.*, Phys. Plasmas **1** (1994) 2229.
[3] E.A. Lazarus *et al.*, Nuclear Fusion **25** (1985) 135.
[4] A.M. Messiaen *et al.*, Nuclear Fusion **34** (1994) 825.
[5] M. Mori *et al.*, Nuclear Fusion **28** (1988) 1892.
[6] G. H. Wolf *et al.*, Plas. Phys. and Control. Nucl. Fusion Res., Proc. 1996 Conf. IAEA, Montreal, Canada, CN-64/02-5.
[7] J. Neuhauser *et al.*, Plas. Phys. Control. Fusion **37**(1995) A37.
[8] Yushmanov *et al.*, Nucl. Fusion **30** (1990) 1999.
[9] C.S. Chang and F. L. Hinton, Phys. Fluids **29** (1986) 3314.
[10] Z. lin *et al.*, Phys. plasmas **2** (1995) 2975.
[11] G.M. Staebler *et al.*, Plasma Phys. Control. Fusion **38** (1996) 1461.
[12] M. Kotchenreuther, Bull Am. Phys. Soc. **37** (1992) 1432.